Please verify that (1) all pages are present, (2) all figures are acceptable, (3) all fonts and special characters are correct, and (4) all text and figures fit within the margin lines shown on this review document. Return to your MySPIE ToDo list and approve or disapprove this submission.

Modeling the laser-induced diffusible resistance process

Michel Meunier,[a,b] Jean-Yves Degorce,[a] Jean-Numa Gillet[a] and François Magny[a]

[a] École Polytechnique de Montréal, Laser Processing Laboratory, C.P. 6079, Succ. Centre-ville, Montréal (Québec), Canada, H3C 3A7
[b] LTRIM Technologies, 440 Blvd. A.-Frappier, suite 140, Laval (Québec), Canada, H7V 4B4

ABSTRACT

Highly accurate resistances can be made by iterative laser-induced local diffusion of dopants from the drain and source of a gateless field effect transistor into its channel, thereby forming an electrical link between two adjacent p-n junction diodes. In this paper we present a complete modeling, which permits to obtain the device characteristics from process parameters. Three-dimensional (3D) temperature calculations are performed from heat diffusion equation using an apparent heat capacity formulation. Melted region determinations are satisfactory compared with in-situ real-time optical measurements of the melted region behavior. Then 3D dopant diffusion profiles are calculated using Fick's diffusion equation. Finally electronic characteristics are obtained from the new tube multiplexing algorithm for computing the I-V characteristic and the device differential resistance. Numerical simulations using our software are satisfactory compared with experimental I-V measurements.

Keywords: *Laser trimming, laser tuned microdevices, laser-induced diffusible resistance, microelectronics, highly accurate resistance, laser process modeling, semiconductor modeling.*

1. INTRODUCTION

Due to the inevitable fabrication process variabilities, analogue microelectronics circuits' functionalities are frequently altered. Trimming techniques have to be used to accurately adjust some microdevices' characteristics. We have recently proposed a new technique, called laser-induced diffusible resistance process, to finely tune analogue microelectronics circuits, which presents the advantages of being very accurate by using very small die area and being easily integrated into any current CMOS processes without additional fabrication steps.[1-5] A patent disclosing the detailed device structure and creation method has been recently accepted.[3] In this paper, after reviewing the principle of the technique, we present a complete modeling of the process.

2. PRINCIPLE OF THE LASER PROCESS

The laser trimming technique, which is schematically shown in Fig. 1, is performed on a device structure consisting of a gateless MOSFET fabricated by a conventional CMOS process.[1-2] For a n-type resistor, the device structure consists of two highly doped n^+ regions formed by implantation inside a p-well, which results in two p-n junctions facing each other. Before the laser trimming operation, the only current that can flow through the device is the p-n junctions' leakage current, which essentially results in an open circuit. Focusing a laser beam on the gap region between the two junctions causes melting of the silicon, which results in dopant diffusion from the highly doped regions to the lightly-doped gap region. Upon removal of the laser light, the silicon solidifies, which leaves the diffused dopants in a new spatial distribution forming an electrical link between the highly doped regions. This laser-diffused link constitutes the tuned microdevice. Tight control of process parameters is necessary to efficiently create these laser tuned microdevices while avoiding damage to adjacent devices and structures. These parameters are the laser spot size, pulse duration, laser power,

Please verify that (1) all pages are present, (2) all figures are acceptable, (3) all fonts and special characters are correct, and (4) all text and figures fit within the margin lines shown on this review document. Return to your MySPIE ToDo list and approve or disapprove this submission.

number of laser expositions and position of the laser spot relatively to the device. By varying the parameters between each laser intervention, we are able to accurately control the device tuning. Scanning electron microscopy and transmission electron microscopy showed that the laser process has no effect on the dielectric multilayers nor on the dielectric/silicon interface.[2,6]

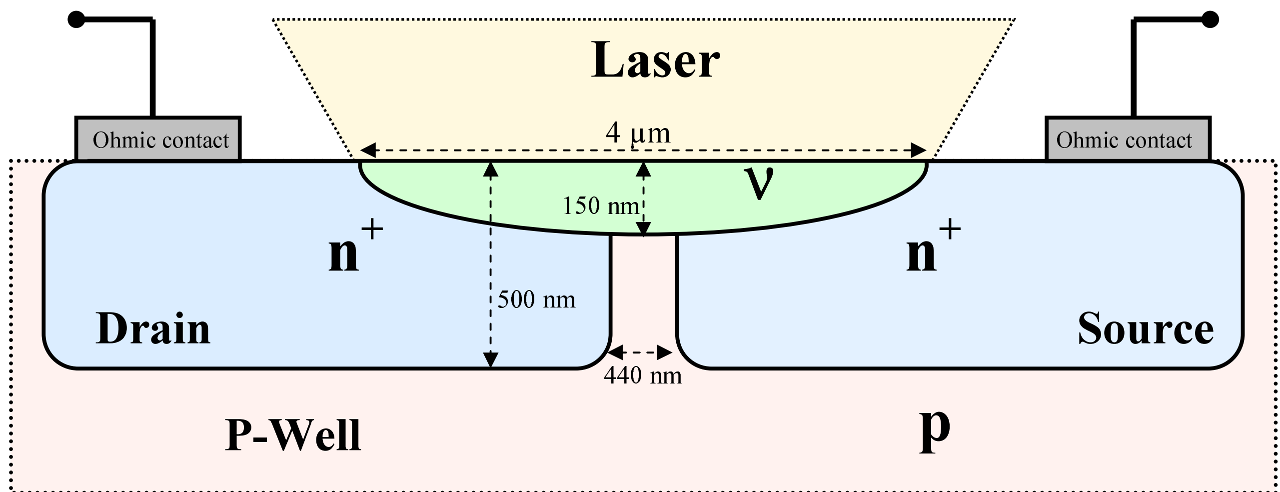

Fig. 1. Schematics of the laser-tuned microdevices' technique.

3. ELECTRICAL PROPERTIES OF THE MICRODEVICES

Figure 2 shows the measured resistance *R* in kΩ of the device as a function of the number of identical pulses (laser power of 4.04 W; pulse width of 80 ns and beam radius of 2 µm) on a chip made with the 0.35 µm technology. After 100 identical pulses, the final resistance value is R=3053.79 Ω. Note that in an industrial application, beam parameters are continuously changed and adjusted using a specially developed algorithm to obtain the desired *R* value.

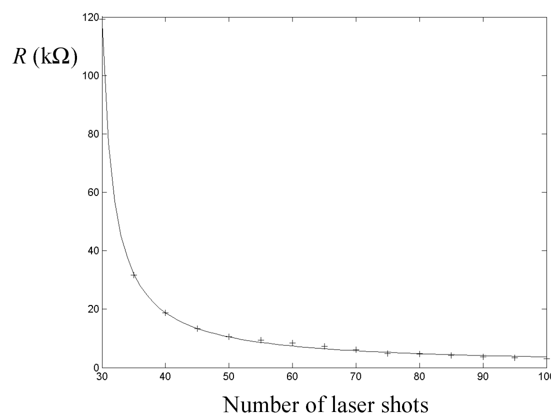

Fig. 2. Typical resistance variation as a function of the number of identical pulses. The conditions are: laser power, 4.04 W; pulse width, 80 ns and beam radius, 2 µm.

Please verify that (1) all pages are present, (2) all figures are acceptable, (3) all fonts and special characters are correct, and (4) all text and figures fit within the margin lines shown on this review document. Return to your MySPIE ToDo list and approve or disapprove this submission.

4. PROCESS MODELING

Modeling this process involves a time-dependent three-dimensional (3D) calculation of the temperature due to the laser irradiation,[7] which is followed by a dopant distribution calculation using the Fick's law. A simple model must include the effects of the laser power, beam waist and exposure time as well as the geometric characteristics of the initial structure. Device characteristics can then be evaluated by solving the three coupled partial differential equations to obtain the 3D distributions of electron and hole concentrations, as well as the electric field in the device presenting a nonuniform dopant distribution. In addition, modeling must also include the possibility of varying the laser beam location and power from pulse to pulse to obtain the desired device characteristics.

Our software is made up of three modeling steps and allows to model the diffused resistor from its fabrication process to its electronic characteristics. In the first step, we use a heat transfer balance equation (modified by incorporating an apparent heat capacity) to determine the temperature distribution of the silicon, which results from the pulsed-laser focused irradiation on the device surface. To verify our model, we successfully compared the numerical results with in situ transient reflectivity measurements. In the second step of the calculation, by using the temperature profile that was previously calculated, the dopant concentration in the diffused resistor is determined by using diffusion equation including segregation. Finally, to obtain the electronic behavior of this new device with the calculated dopant profile, the semiconductor equations are solved using the new tube multiplexing algorithm.

5. THREE-DIMENSIONAL SIMULATION OF THE MELTED-ZONE DYNAMICS

The calculation of the total spatial and temporal behavior of the temperature distribution within the solid and liquid material can be only numerically obtained. Modeling of the related heat problems has been reported in several papers[8-10] but none of them dealt with a focused laser beam or two-material problem. We have developed an exhaustive numerical approach of a two-phase transient temperature field within silicon substrate covered by a silicon dioxide thin film irradiated by a focused visible laser with pulse durations of the order of some tens of ns. All material parameters are taken to be temperature dependent. Oxide layer on the irradiated surface of silicon is usually expected to remain solid during laser processing,[9,11] which imposes that the maximum temperature always remains between the melting point of silicon and silicon dioxide.

Usually the thermal field induced by a pulsed laser irradiation into bulk silicon is not only due to heat diffusion, but also depends on the penetration depth of the laser light. Laser-induced heating changes the optical properties of the material owing to their temperature dependence. The dissipated-energy distribution is therefore calculated from the Maxwell equations,[12] and with common assumptions[13] the problem can be considerably simplified. In a cylindrical (r, z) symmetry, the time-dependant source term in the heat equation can be written as

$$Q(z) = [1 - R(T(r, z=0))]I(r,t)f(z) \tag{1}$$

where $f(z)$ is solution of the Beer-Lambert equation given by

$$\frac{\partial f(z)}{\partial z} = \alpha(T,\lambda)f(z), \tag{2}$$

$I(r)$ is the intensity of the Gaussian heating laser beam and $R(\lambda, T(z=0))$ is the temperature dependent optical reflectivity for the considered wavelength λ. Optical absorption is characterized by a typical length $l_\alpha = \alpha^{-1}$ where $\alpha(T)$ is the temperature-dependent optical absorption coefficient. For surface absorption, l_α is small compared to the heat diffusion length $l_T \approx 2\sqrt{Dt}$ where D is the thermal diffusivity and t is the interaction time. In this case, either a point source[14] or an infinite source[15, 16] lead to an approximate analytical solution of the heat equation. For laser pulses of some tens of ns, the heat-diffusion length in silicon is typically of few µm while the optical absorption length is of the order of 10 nm,

Please verify that (1) all pages are present, (2) all figures are acceptable, (3) all fonts and special characters are correct, and (4) all text and figures fit within the margin lines shown on this review document. Return to your MySPIE ToDo list and approve or disapprove this submission.

which means that during the first stages of irradiation the energy balance near the Si surface must include both heat-diffusion and source terms. Any realistic model of laser-mater interaction for annealing process must be carried out through 3D calculations including all temperature dependencies of the material parameters, i.e. heat capacity C, thermal conductivity κ, mass density ρ, α and R.

We have included in the simulation a transparent oxide layer (0.5 µm of SiO_2) over the silicon flat surface, in order to take into account that real devices are covered by dielectric multilayers. This layer induces discontinuous changes in the physical properties of the material. Since the silicon melting must occur without SiO_2 melting, the surface temperature must remain in a small range of temperature between the melting temperature of Si, $T_{m\mathrm{Si}}$ = 1685 K,[17] and that of SiO_2, $T_{m\mathrm{SiO2}}$ = 1980 K.[17] Moreover the presence of this solid layer onto the upper silicon surface enables us to ignore convection phenomena as it was verified by Whelan et al.[11]

The axis-symmetry mathematical modelling includes (i) optical absorption of the focused laser (λ =532 nm), (ii) heat diffusion in the two materials with a phase change in the silicon substrate and (iii) reflectivity of a probing laser (λ =623 nm). All physical parameters are taken to be temperature dependent. While melting is taking place, the material is divided into two parts: (i) solid and (ii) melt with different thermal properties. A difficulty arises because the boundary between solid- and melted silicon moves with time and complex boundary conditions have to be considered at the interface. Nevertheless, rather than dividing the material into two subdomains, it is possible to obtain a single equation, which will be applied through the entire domain. No special reference to either solid or melted silicon is necessary.

Temperature distribution induced by the laser-radiation absorption within the substrate can be calculated using the heat equation for the particular geometry and the substrate under consideration. $T(r, z, t)$ is a function of both spatial and time coordinates. With fixed laser parameters, the temperature depends on (i) optical absorption within the irradiated zone, (ii) the transport of heat out of this zone and (iii) change of phase enthalpies. In Si and SiO_2 the heat equation can be written in a coordinate system that is fixed with the laser beam as

$$\rho(T)c(T)\frac{\partial T}{\partial t} = \nabla\big(\kappa(T)\nabla T\big) + Q_p + L(Si) \tag{3}$$

where $\rho(T)$ is the mass density, $c(T)$ the specific heat at constant pressure, $\kappa(T)$ the thermal conductivity in both materials and L the silicon latent heat of melting. The transmitted energy per unit of volume and time is $\alpha(T)I(r, z)$ where the absorption coefficient $\alpha(T, \lambda)$ depends on both temperature and heating laser wavelength. Because of this temperature dependence, the optical properties of the material become inhomogeneous under laser irradiation. Using the classical enthalpy model [21], it is possible to obtain a single equation for the entire bulk silicon. We obtain from Eq. (3):

$$\frac{\partial \Delta H(r,z,t)}{\partial t} = \nabla\big(\kappa(T)\nabla T\big) + Q_p(r,z,t) \tag{4a}$$

where ΔH is the total enthalpy expressed by

$$\Delta H(T) = \int_{T_\infty}^{T} \rho(T)c(T)dT + U(T-T_m)L(Si) \tag{4b}$$

This term keeps track of the total energy accumulated in one point of the material. If T_∞ is the temperature far from the processed area, and $U(T-T_m)$ is a Heaviside function, which is zero if $T<T_m$ and unity if $T>T_m$, using the chain rule:

$$\frac{\partial \Delta H(T)}{\partial T}\frac{\partial T}{\partial t} = \nabla\big(\kappa(T)\nabla T\big) + Q_p(r,z,t) \tag{5}$$

However, the temperature derivative of the enthalpy becomes infinite at the melting temperature T_m hence:

$$\frac{\partial \Delta H}{\partial T} = \rho(\mathrm{T})\mathrm{c}(\mathrm{T}) + \delta(T-T_m)L \tag{6}$$

where $\delta(T-T_m)$ is the Dirac function. Now, we introduce an apparent specific heat equation

$$\rho(T)c_e(T) = \rho(T)c(T) + \delta(T-T_m)\rho(T)L \tag{7}$$

Please verify that (1) all pages are present, (2) all figures are acceptable, (3) all fonts and special characters are correct, and (4) all text and figures fit within the margin lines shown on this review document. Return to your MySPIE ToDo list and approve or disapprove this submission.

In order to bypass the singularity problem at the melting temperature, we assumed that the phase change occurs over a small temperature interval ΔT = 5 K. A second difficulty arises due to the steep change of the silicon thermal conductivity at the melting temperature. In order to avoid numerical instabilities, this thermal conductivity is expressed using the Kirchhoff transformation:

$$\Theta_{Si}(T) = \int_{T_\infty}^{T} \frac{\kappa(T)}{\kappa(T_\infty)} dT \tag{8}$$

In term of Kirchhoff temperatures, Θ_{Si} and Θ_{SiO2}, the heat equation system has the form:

$$\frac{1}{D_{Si}(\Theta)} \frac{\partial \Theta_{Si}(T,t)}{\partial t} = \nabla^2 \Theta_{Si}(T) + \frac{Q_p(\Theta_{Si},t)}{\kappa_{Si}(T_\infty)} \tag{9a}$$

$$\frac{1}{D_{SiO_2}(\Theta)} \frac{\partial \Theta_{SiO_2}(T,t)}{\partial t} - \nabla^2 \Theta_{SiO_2}(T) = 0 \tag{9b}$$

where $D=\kappa(\Theta)/\rho(\Theta)c_e(\Theta)$. These equations can be solved by a finite-element calculation.

We performed numerical experiments on silicon covered by a 0.5 µm oxide layer and irradiated by a focused laser. The knowledge of the maximum laser-induced temperature rise is of great importance since it must remains below T_{mSiO2} = 1980 K. With a focused laser, the maximum surface temperature always occurs at the center of the laser beam (r = 0, z = 0). The temporal behaviors at the center and two other points located on the silicon surface are compared in Fig. 3. Since the center point receives the maximum amount of laser beam energy, it melts first and is the last to solidify as seen in Fig. 3. $T(r = 0, z = 0)$ reaches melting within a time τ_m after the onset of the laser energy. Subsequently, $T(r = 0, z = 0)$ increases at a lower pace as the absorbed laser light energy is spent not only on heating but also on melting. Moreover the steep increase of optical reflectivity at the melting temperature amplifies this phenomenon. The maximum temperature is reached approximately (dependent on the pulse shape) at the end of the laser pulse: τ_l, then the silicon cools and solidifies within a time τ_s. We deduce from the different times (τ_l, τ_s, τ_m) and Si melting duration: $\Delta t_m = \tau_s - \tau_m$.

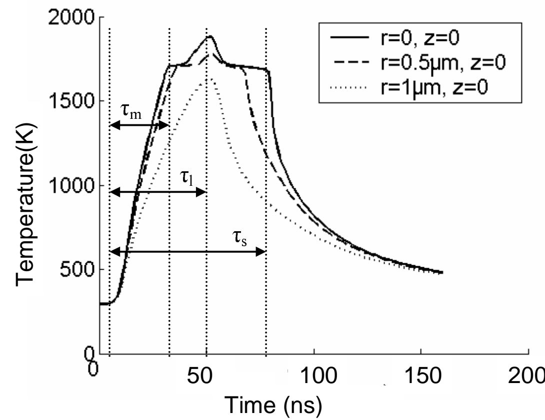

Fig. 3. Calculated temporal behaviour of the temperature at the center point (r = 0, z = 0) and two other points of the silicon irradiated surface, induced by a single Gaussian laser pulse of maximum laser intensity: I_0 = 1.35 10^7 W/cm^2, laser beam radius: r_0 = 0.85 µm, and pulse duration: τ_l = 40 ns (from 10 to 50 ns).

Please verify that (1) all pages are present, (2) all figures are acceptable, (3) all fonts and special characters are correct, and (4) all text and figures fit within the margin lines shown on this review document. Return to your MySPIE ToDo list and approve or disapprove this submission.

The temperature distributions on the irradiated surface $T(r, z = 0)$ and along the z axis $T(r = 0, z)$ are plotted in Fig. 4 for different times in the vicinity of the pulse duration. We can deduce for each time, the molten radius and molten depth as their maximum values occurred approximately at the end of the pulse (depending on the pulse shape). We can observe that r_{melt} is one order of magnitude higher than and z_{melt}, because for short laser pulses, the surface temperature primarily depends on laser beam intensity profile with a characteristic length given by the 1/e radius r_0 of the heating laser beam, while along the z axis, the temperature distribution depends on heat diffusion with a typical length of $l_T \approx 2\sqrt{Dt}$.

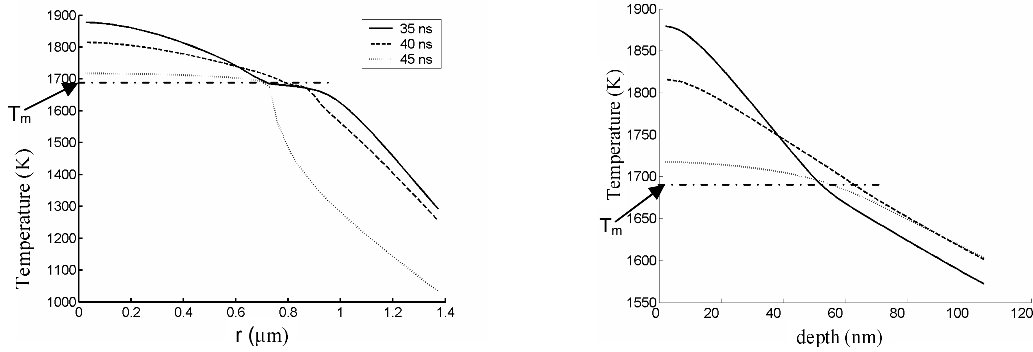

Fig. 4. (a) Surface temperature distribution $T(r, z = 0)$ and (b) temperature distribution along the z axis induced by a Gaussian laser pulse at different times around the pulse duration of $\tau_l = 40$ ns

6. MELTED-DYNAMIC SIMULATIONS VERSUS TRANSIENT REFLECTIVITY MEASUREMENTS

In order to compare calculated transient surface temperature distribution with experimental data, we carried out experiments of transient reflectivity measurement of a cw HeNe probe laser (radius = 3 µm) aligned collinearly with the heating Nd:YAG laser (radius = *0.85 µm)*. Since the reflectivity depends on both temperature and phase state, reflected intensity of the HeNe probe laser is a good probing indicator of the laser-annealing process.[18,10] As the laser irradiates silicon, the surface reflectivity $R(T, \lambda=633nm)$ evolves linearly [19,20] with temperature from the solid Si value[21,20] to the melting temperature value[20] where silicon becomes essentially metallic, resulting in a sharp optical reflectivity increase. The choice of the red wavelength for the probing light is justified by the large difference between liquid and solid reflectivity coefficients which improves the accuracy of the measurement. The recorded reflected intensity is indicated in Fig. 5. In order to assess the validity of our numerical model, using the surface temperature distribution, we calculated numerically the reflected power at each time during the heating-melting-cooling process by using

$$P_{reflected}(t) = \int_0^{r\max} R(\lambda = 633nm, T(z=0))\, e^{-\left(r/r_{0HeNe} \right)^2} dr \qquad (10)$$

where $P_{reflected}$ denotes a non-dimensional reflected light power and r_{0HeNe} is the 1/e radius of the Gaussian HeNe laser beam. Experimental and numerical data are in good agreement for different pulse durations suggesting strongly that our calculations represent adequately the focused laser process inducing both heating and phase changes.

Please verify that (1) all pages are present, (2) all figures are acceptable, (3) all fonts and special characters are correct, and (4) all text and figures fit within the margin lines shown on this review document. Return to your MySPIE ToDo list and approve or disapprove this submission.

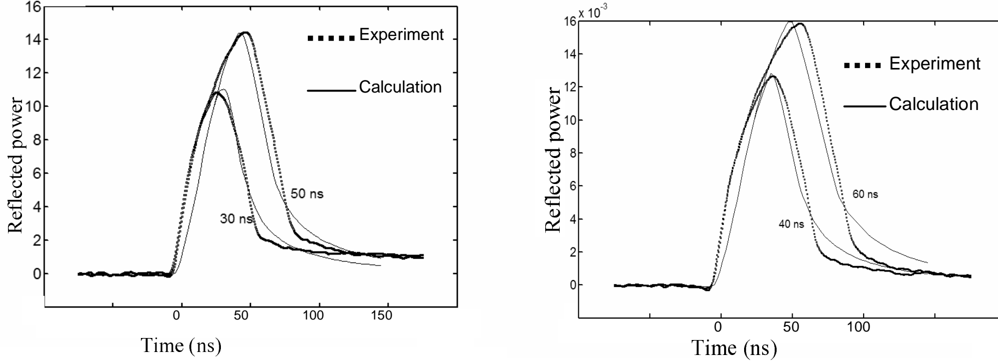

Fig. 5. The doted curves are derived from measurements. Calculated curves (solid curves) are deduced from Eq. (10). Each experimental curve is obtained by averaging ten identical transient reflected power measurements.

7. THREE-DIMENSIONAL MODELING OF DOPANT DIFFUSION AND SEGREGATION

Diffusion and segregation of impurity species concurrently occur in inhomogeneous materials. The solid-liquid moving interface in the material is an abrupt boundary, which separates solid and liquid silicon during solidification. Segregation occurs at this interface, while diffusion takes place within the liquid silicon. Segregation is driven by the spatial variation of the Gibbs free energy, which depends on the mixing entropy of the dopant species. The following equations are derived from thermodynamic basis:[22]

$$\frac{\partial C}{\partial t} = \nabla \cdot \left[D \left(\nabla C - C \frac{\nabla C^{eq}}{C^{eq}} \right) \right] \tag{11}$$

where $\nabla C^{eq} / C^{eq}$ depends on the constant segregation coefficient $k = C_S^{eq} / C_L^{eq} \leq 1$, which is defined as the ratio of the equilibrium concentrations in the solid and the liquid, respectively.[22,23]

Figure 6 shows the boron profile in a longitudinal cross-section of a p+-π-p+ device with a 1 µm original gap. In Fig. 6(a) we see the implanted Gaussian profile of the drain and the source with a maximal B concentration of $N_A = 1.4 \times 10^{19}$ cm^{-3} at a depth of $y = 30$ nm and the abrupt dopant decrease in the 1 µm gap with a low B concentration of $N_A = 10^6$ cm^{-3}. While segregation is considered in this calculation, this effect for Boron is relatively weak because k = 0.8 is closed to one.[23] The Boron profile, which results from dopant diffusion into the gap after laser trimming, is given in Fig. 6(b) for a longitudinal cross-section, which is located at the center of the melted zone with the transverse coordinate $z = 0$. We still see the implanted Gaussian profile at the device extremities with the longitudinal coordinates $x = 0$ (left-hand side) and $x = 4.8$ µm (right-hand side), because the melted zone has a maximal diameter of $2\ r_{max} = 2.1$ µm and is centered at $x = 2.4$ µm. Close to the device surface with $y = 0$ and by moving the eyes from $x = 2.4 - r_{max} = 1.35$ µm at the left-hand side and from $x = 2.4 + r_{max} = 3.45$ µm at the right-hand side to the device center at $x = 2.4$ µm, we note a smooth decrease of the dopant profile from the concentration of 1.4×10^{19} cm^{-3} to that of 5×10^{18} cm^{-3}, which is due to dopant diffusion in the gap. At lower depths the transition in the gap becomes more abrupt and, for depths lower than the maximal melt depth of $y = 95$ nm, the unaffected B concentration of 10^6 cm^{-3} in the gap center is obtained. With these results we can generate a 3-D profile of the B concentration due to the laser induced dopant diffusion.

Please verify that (1) all pages are present, (2) all figures are acceptable, (3) all fonts and special characters are correct, and (4) all text and figures fit within the margin lines shown on this review document. Return to your MySPIE ToDo list and approve or disapprove this submission.

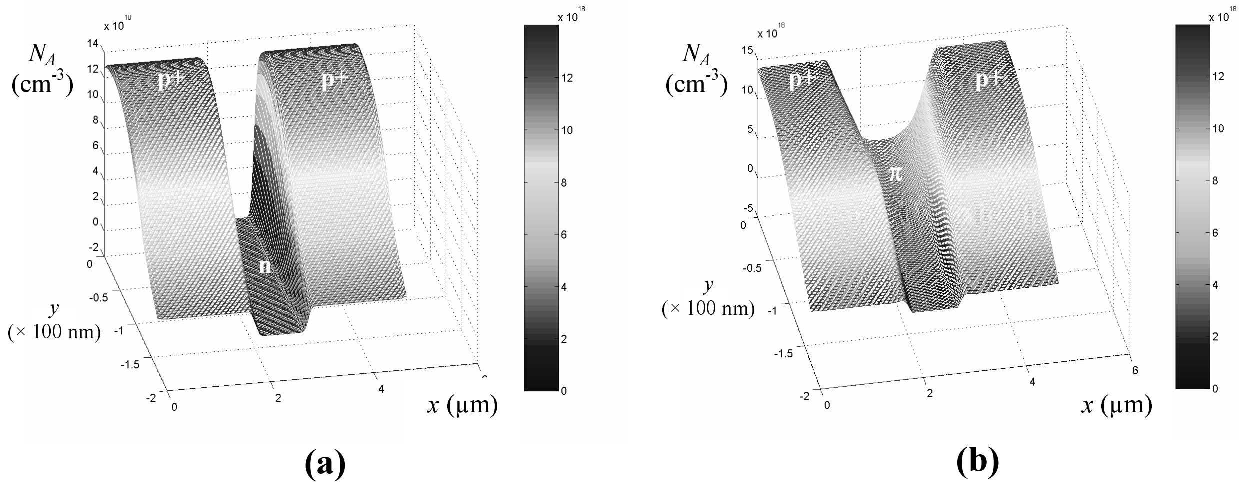

Fig. 6. Dopant profiles: (a) as implanted with a maximal concentration of $N_A = 1.4 \times 10^{19}$cm^{-3}, (b) after dopant diffusion through the gap for the longitudinal cross-section located at the melted-basin center with the transverse coordinate $z = 0$.

8. THREE-DIMENSIONAL MODELING OF THE MICRODEVICE ELECTRONIC BEHAVIOR

The device electronic behavior is determined from its current-voltage (I-V) characteristic, which usually is linear at low voltages and saturates at higher voltages, where high electric fields affect carrier mobility.[24] The device I-V curve is usually obtained by solving a system of 3 coupled second-order partial differential equations with a finite-element method. Due to the need of 3-D finite elements, this device cannot be modeled with this classical method owing to its prohibitive computational cost and memory limitation. To avoid this problem, we introduced a novel tube multiplexing algorithm (TMA) to rapidly compute the I-V curve of the 3-D resistor as a function of the drain-source voltage drop V_D and operation temperature T. Details of this new approach will be presented elsewhere[25] and only the major points will be given here. In our TMA we divided the 3-D resistor into a number of $K \times W$ tubes with parallelepiped shapes. The tubes are spatially multiplexed because we can prove mathematically that the electric field in any tube only depends on the tube longitudinal coordinate x, assuming that the dopant concentration of the tube is independent of the depth y and transverse coordinate z.[25] Figure 7 shows a longitudinal cross-section of one p+-π-p+ example device, which is located at the center of the melted zone with the transverse coordinate $z = 0$. There are $K + 1 = 11$ tube boundaries in the y direction and $W + 1 = 6$ in the z direction, so that the number of tubes used by the TMA is $KW = 50$. The dopant profiles at $z = 0$ and $z = 1.05$ μm are given in Fig. 6(b) and 6(a), respectively. We apply the boundary conditions for the electrostatic potential ψ on two transverse cross-sections with a depth of $y_f = 97$ nm located in the left- and right- hand sides of the 3-D device. y_f is a fit parameter, which is larger than the maximal melt depth of 95 nm but smaller than the n-well depth because the n-well is biased to a potential $V_{n\text{-}well} \geq V_D$. We also consider that there is no current density when $z \geq r_{max}$.

Please verify that (1) all pages are present, (2) all figures are acceptable, (3) all fonts and special characters are correct, and (4) all text and figures fit within the margin lines shown on this review document. Return to your MySPIE ToDo list and approve or disapprove this submission.

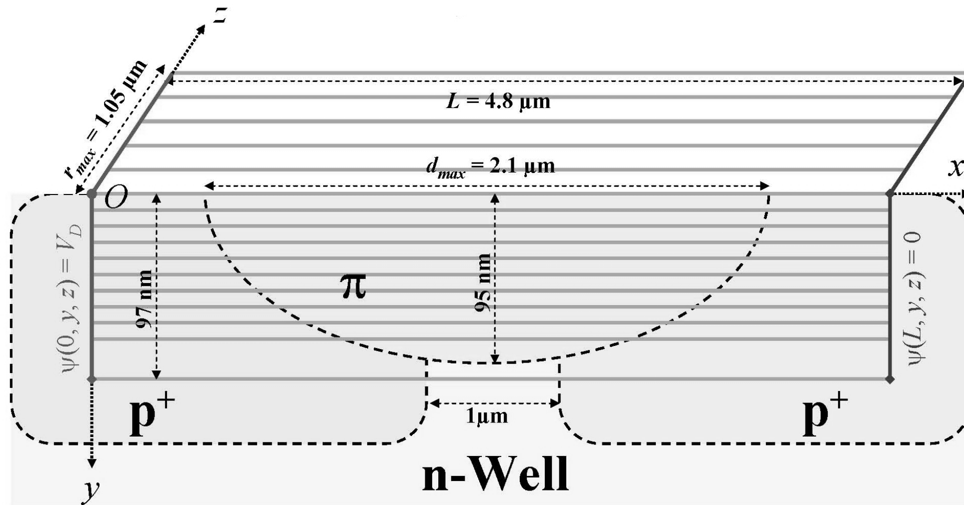

Fig. 7. Longitudinal cross-section of a p+-π-p+ device, which is located at $z = 0$. The 3-D device is divided into $KW = 50$ tubes, where $K + 1 = 11$ and $W + 1 = 6$ are the numbers of tube boundaries in the y and z directions, respectively.

This new algorithm is fast because the 3-D device I-V curve is obtained by solving a system of 3 coupled first-order ordinary differential equations (ODE) for each tube, which allows a fast convergence in contrast to the classical method. The tube currents are also coupled each other because the TMA considers, for each tube, diffusion currents in the directions y and z that are perpendicular to the tubes, as shown in Fig. 7. Moreover, to reduce the error on the carrier mobility $\mu_{kw}(x)$, which depends on x in each tube indexed by $k = 1, \ldots, K$ and $w = 1, \ldots, W$, an iterative error-reduction process[26] is coded in the TMA in order to solve the 3-ODE system with a high accuracy. Also the TMA presents a good convergence although doping and electrical field suffer of large numerical fluctuations. As a result, for a given voltage V_D and temperature T, the total drain current I_D, which is equal to the summation of the 50 tube currents multiplied by 2, is obtained with a low error although the preset number of 50 tubes is moderate. The 50 tube currents are computed by using the multiplexed solutions for the carrier (hole or electron) concentration $n_{kw}(x)$, electric field $E_{kw}(x)$ and potential $\psi_{kw}(x)$, which are obtained by the TMA for each tube. Then the process is repeated for different voltages V_D.

Figure 8 presents the experimental results for a device process with 100 identical pulses (see conditions in figure captions of Fig. 2). The complete I-V curve of a p^+-π-p^+ example device was computed for V_D in a range from 0 to 5 V at $T = 300$ K. As shown in the Fig. 8, the computed results for that device are given by circles (o) and present a very good agreement with the experimental results given by crosses (+). The TMA can also be repeated for different temperatures T, so that a number of I-V curves are obtained as a function of T.[27] By using a curve-fitting algorithm, we can determine, with an error lower than 1 %, a relationship between the computed values of I_D and doublet (V_D, T), which is $I_D = a(T)\{1\text{-}\exp[-b(T)V_D]\}$, where $a(T)$ and $b(T)$ are fit functions of T, as shown in Fig. 8(a). The resistance-voltage (R-V) curve is then computed by simple division, $R = V_D/I_D$, and presents a good agreement with the experimental curve, as shown in Fig. 8(b). As a consequence, the mathematical expression of the drain current I_D of a semiconducting resistor fabricated by laser-induced dopant diffusion is similar to the emitter current expression of a bipolar transistor and drain current of a MOSFET in subthreshold regime [27-28].

Please verify that (1) all pages are present, (2) all figures are acceptable, (3) all fonts and special characters are correct, and (4) all text and figures fit within the margin lines shown on this review document. Return to your MySPIE ToDo list and approve or disapprove this submission.

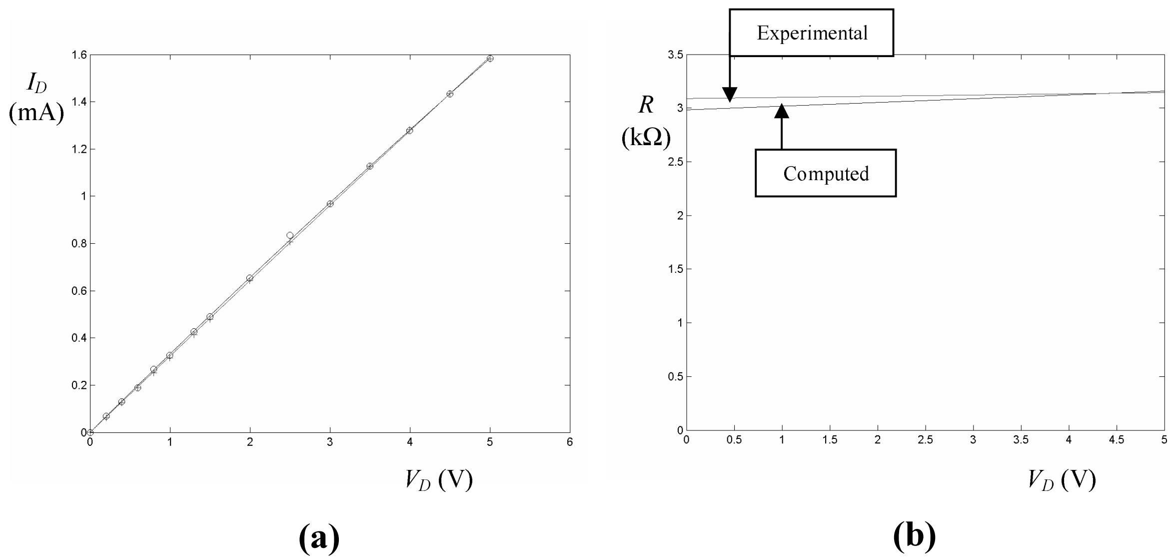

Fig. 8. Computed and experimental I-V curves (a) and R-V curves (b). I-V curves are given in (a), where the circles (o) and crosses (+) are computed and experimental results, respectively, which are fitted by the two curves; computed and experimental R-V curves are given in (b).

9. CONCLUSIONS

Highly accurate resistors compatible with CMOS technology can be easily made by laser inducing dopant diffusion. These new microdevices have very linear I-V curves at the usual microelectronics operating voltages and present nonlinear behavior due to carrier velocity saturation at higher voltages. A complete simulation of the process has been performed to obtain the electronic characteristics of the device from the laser process parameters. New algorithm approaches to obtain both the 3D temperature distribution in the solid and liquid phases induced by a focused laser using an apparent heat capacity formulation and the I-V curves using a new tube multiplexing algorithm have been introduced and successfully compared with experimental results. This modeling constitutes the basic tool to develop an efficient control of the process.

ACKNOWLEDGMENTS

The authors are grateful to Jean-Paul Lévesque and Hugo St-Jean for technical assistance and to Alain Lacourse for stimulating discussions. We also acknowledge the financial contribution from NSERC of Canada.

SPIE USE, V. 2 5339A-39 (p.10 of 11) / Color: No / Format: A4/ AF: A4 / Date: 2004-02-22 20:02:01

Please verify that (1) all pages are present, (2) all figures are acceptable, (3) all fonts and special characters are correct, and (4) all text and figures fit within the margin lines shown on this review document. Return to your MySPIE ToDo list and approve or disapprove this submission.

REFERENCES

[1] M. Meunier, Y. Gagnon, A. Lacourse, Y. Savaria and M. Cadotte, "A novel laser trimming process for microelectronics," Proc. SPIE **4274**, 385-392 (2001).

[2] M.Meunier, M. Cadotte, M. Ducharme, Y. Gagnon and A. Lacourse, "Laser induced diffusible resistance: device characterization and process modeling," Proc. SPIE **4637**, 75-81 (2002).

[3] M. Meunier, Y. Gagnon, Y. Savaria, A. Lacourse and M. Cadotte, A New Laser Trimming Process for Microelectronics," Appl. Surf. Sci. **186**, 52-56 (2002).

[4] Y. Gagnon, M. Meunier and Y. Savaria, "Method and Apparatus for Iteratively and Selectively Tuning the Impedance Integrated Semiconductor Devices Using a Focused Heating Source," US Patents 09/332,059 and PCT # 06042-002-WO-1 by LTRIM Technologies Inc. (2001).

[5] M. Meunier, M. Cadotte and M. Ducharme "Laser tuned silicon microdevices for analogue microelectronics," Riken Review, Vol. 50, pp. 53-56 (2003).

[6] M. Meunier, M. Ducharme , J-Y. Degorce, Y. Liao and A. Lacourse, "Laser induced local modification of silicon microdevices: a new technique for tuning analogue microelectronics," Proc. SPIE **5147**, 316-321 (2003).

[7] A. Van der Ziel, "Space-Charge-Limited Solid-State Diode," Semiconductors and Semimetals, Vol.14, pp.195-247 (1979).

[8] T. Rantala and J. Levoska, "A numerical simulation method for the laser-induced temperature distribution," J. Appl. Phys. **65**, 4475 (1988).

[9] X. Zang, J.R. Ho and C.P. Grigoropoulos, "Ultra-shallow p^+-junction formation in silicon by excimer laser doping: a heat and mass transfer perspective," Int. J. Heat Mass Transfer **39**, 3835 (1996).

[10] R.F. Wood and G.E. Giles, "Macroscopic theory of pulsed-laser annealing. I. Thermal transport and melting," Phys. Rev. B **23**, 2923 (1981).

[11] S. Whelan, A. La Magna, V. Privitera, G. Mannino, M. Italia and C. Bongiorno, "Dopant redistribution and electrical activation in silicon following ultra-low energy boron implantation and excimer laser annealing," Phys. Rev. B **67**, 075201 (2003).

[12] M. Born and E. Wolf, *Principles of optics* (Pergamon, Oxford, UK, 1980).

[13] D. Bauerle, *Laser processing and chemistry*, 3rd ed. (Springer, Berlin, 2000).

[14] J.-Y. Degorce, A. Saucier and M. Meunier, "A simple analytical method for the characterization of the melt region of a semiconductor under focused laser irradiation," Appl. Surf. Sci. **208-209**, 267-271 (2003).

[15] H.S. Carslaw and J.C. Jaeger, *Conduction of heat in solids* (Clarendon Press, Oxford, UK, 1988).

[16] V.N. Tokarev and A.F.H. Kaplan, "An analytical modeling of time dependent pulsed laser melting," J. Appl. Phys. 86, 2836 (1999).

[17] M. Thompson, G.J. Galvin, J.W. Mayer, P.S. Peercy and J.M. Poate, "Melting Temperature and Explosive Crystallization of Amorphous Silicon during Pulsed Laser Irradiation," Phys. Rev. Lett. **52**, 2360-2363 (1984).

[18] G.E. Jellison, D.H. Lowndes, D.N. Masburn and R.F. Wood, "Time-resolved reflectivity measurements on silicon and germanium using a pulsed excimer KrF laser heating beam**,"** Phys. Rev. B **34**, 2407-2415 (1986).

[19] J. Heller, J.W. Barthe, C. C. Poon and C. Tam, "Temperature dependence of the reflectivity of silicon with surface oxide at wavelengths of 633 and 1047 nm," Appl. Phys. Lett. **75**, 43 (1999).

[20] N. Chaoui, J. Siegel, J. Solis and C. N. Alfonso, "Reflectivity of crystalline Ge and Si at the melting temperature measured in real time with subnanosecond temporal resolution," J. Appl. Phys **89**, 3763 (2001).

[21] G.E. Jellison and F.A. Modine, "Optical functions of silicon between 1.7 and 4.7 eV at elevated temperatures," Phys. Rev. B **27**, 7466 (1983).

[22] H.M. You, U. Gosele and T.Y. Tan, "Simulation of the transient indiffusion-segregation process of triply negatively charged Ga vacancies in GaAs and AlAs/GaAs superlattices," J. Appl. Phys. **74**, 2461 (1993).

[23] R.F. Wood, J.R. Kiripatrick and G.E. Giles, "Macroscopic theory of pulsed-laser annealing. II. Dopant diffusion and segregation," Phys. Rev. B **23**, 5555 (1981)

[24] A. Schenk, *Advanced Physical Models for Silicon Device Simulation* (Springer, Vienna, 1998), chap. 1, pp. 1-125.

[25] J.-N. Gillet and M. Meunier, manuscript in preparation (2004).

[26] J.-N. Gillet and Y. Sheng, "Multiplexed computer-generated holograms with irregular-shaped polygonal apertures and discrete phase levels," J. Opt. Soc. Am. A **19**, 2403-2413 (2002).

[27] J.-N. Gillet and M. Meunier, "New algorithm for fast computing the I-V characteristics of n^+-ν-n^+ semiconductor devices," 11th Canadian Semiconductor Technology Conference, 18-22 Aug. 2003, Ottawa, p. 155.

[28] S. M. Sze, *Semiconductor Devices. Physics and Technology*, 2nd ed. (Wiley, New York, 2001), chap. 5 and 6, pp. 130-223.

SPIE USE, V. 2 5339A-39 (p.11 of 11) / Color: No / Format: A4/ AF: A4 / Date: 2004-02-22 20:02:01